

1 **Origin of elemental carbon in snow from Western Siberia**
2 **and northwestern European Russia during winter–spring**
3 **2014, 2015 and 2016**

4
5 **Nikolaos Evangeliou^{1,*}, Vladimir P. Shevchenko², Karl Espen Yttri¹, Sabine**
6 **Eckhardt¹, Espen Sollum¹, Oleg S. Pokrovsky^{3,4}, Vasily O. Kobelev⁵, Vladimir B.**
7 **Korobov⁶, Andrey A. Lobanov⁵, Dina P. Starodymova², Sergey N. Vorobiev⁷,**
8 **Rona L. Thompson¹, Andreas Stohl¹**

9
10 ¹ NILU - Norwegian Institute for Air Research, Department of Atmospheric and Climate
11 Research (ATMOS), Kjeller, Norway.

12 ² Shirshov Institute of Oceanology, Russian Academy of Sciences, Nakhimovsky prospect 36,
13 117997 Moscow, Russia.

14 ³ Geosciences Environment Toulouse, UMR 5563 CNRS, University of Toulouse, 14 Avenue
15 Edouard Belin, 31400, Toulouse, France.

16 ⁴ N. Laverov Federal Center for Integrated Arctic Research, Russian Academy of Science,
17 Sadovaya street, 3, 163000, Arkhangelsk, Russia.

18 ⁵ Arctic Research Center of the Yamalo-Nenets autonomous district, Vos'moy proezd, NZIA
19 building, 629730, Nadym, Yamalo-Nenets autonomous district, Russia.

20 ⁶ North-Western Branch of Shirshov Institute of Oceanology, Russian Academy of Sciences,
21 Naberezhnaya Severnoy Dviny 112/3, 163061, Arkhangelsk, Russia.

22 ⁷ BIO-GEO-CLIM Laboratory, Tomsk State University, 36 Prospect Lenina, 634050, Tomsk,
23 Russia.

24
25 *Correspondence to: N. Evangeliou, NILU - Norwegian Institute for Air Research,
26 Department of Atmospheric and Climate Research (ATMOS), Kjeller, Norway
27 (Nikolaos.Evangeliou@nilu.no)

28

29 **Abstract**

30 Short-lived climate forcers have been proven important both for the climate and human
31 health. In particular, black carbon (BC) is an important climate forcer both as an aerosol and
32 when deposited on snow and ice surface, because of its strong light absorption. This paper
33 presents measurements of elemental carbon (EC; a measurement-based definition of BC) in
34 snow collected from Western Siberia and northwestern European Russia during 2014, 2015
35 and 2016. The Russian Arctic is of great interest to the scientific community due to the large
36 uncertainty of emission sources there. We have determined the major contributing sources of
37 BC in snow in Western Siberia and northwestern European Russia using a Lagrangian
38 atmospheric transport model. For the first time, we use a recently developed feature that
39 calculates deposition in backward (so-called retroplume) simulations allowing estimation of
40 the specific locations of sources that contribute to the deposited mass.

41 EC concentrations in snow from Western Siberia and northwestern European Russia
42 were highly variable depending on the sampling location. Modelled BC and measured EC
43 were moderately correlated ($R = 0.53 - 0.83$) and a systematic region-specific model
44 underestimation was found. For EC sampled in northwestern European Russia the
45 underestimation by the model was smaller (fractional bias, $FB > -100\%$). In this region, the
46 major sources were transportation activities and domestic combustion in Finland. When
47 sampling shifted to Western Siberia, the model underestimation was more significant ($FB < -$
48 100%). There, the sources included emissions from gas flaring as a major contributor to snow
49 BC. The accuracy of the model calculations was also evaluated using two independent
50 datasets of BC measurements in snow covering the entire Arctic. The model reproduced snow
51 BC concentrations quite accurately, although small discrepancies occurred mainly for samples
52 collected in springtime. Nevertheless, EC concentrations in snow presented here are about
53 20% lower than previously reported ones in Western Siberia and northwestern European
54 Russia.

55

56 **1 Introduction**

57 Black carbon (BC) is the strongest light-absorbing component of atmospheric aerosol
58 and is formed by the incomplete combustion of fossil fuels, biofuels, and biomass (Bond et
59 al., 2013). It is emitted directly into the atmosphere in the form of fine particles. BC is a major
60 component of “soot”, a complex light-absorbing mixture that also contains organic carbon
61 (OC) (Bond et al., 2004). Combustion sources emitting BC include open biomass burning
62 (forest, savanna, agricultural burning), residential biofuel combustion, diesel engines for
63 transportation or industrial use, industrial processes and power generation, or residential coal
64 combustion (Liu et al., 2011; Wang et al., 2011).

65 BC is important on a global perspective because of its impacts on human health and on
66 climate. As a component of fine particulate matter (PM_{2.5}), it is associated with negative
67 health impacts, including premature mortality (Lelieveld et al., 2015; Turner et al., 2005). It
68 absorbs solar radiation, has a significant impact on cloud formation and, when deposited on
69 ice and snow, it accelerates ice melting (Hansen and Nazarenko, 2004). BC has a lifetime that
70 can be as long as 9–16 days (Bond et al., 2013). After its emission, BC can travel over long
71 distances (Forster et al., 2001; Stohl et al., 2006) and reach remote areas such as the Arctic.
72 Arctic land areas are covered by snow in winter and spring, while the Arctic Ocean is partly
73 covered by ice. Sea ice has a much higher albedo (≈ 0.5 – 0.7) compared to the surrounding
74 ocean (≈ 0.06), thus presence of sea ice reduces the heat uptake of the ocean. Snow has an
75 even higher albedo than sea ice and can reflect as much as 90% of the incoming solar
76 radiation (Brandt et al., 2005; Singh and Haritashya, 2011). BC deposited on ice lowers its
77 albedo, increases heat uptake by sea ice, accelerates its melting, and therefore decreases
78 surface albedo both directly and indirectly.

79 Hegg et al. (2009) reported that snow in the Arctic often contains BC at concentrations
80 between 1 and 30 ppb, which can cause a snow albedo reduction of 1–3% in fresh snow and
81 another 3–9% as snow ages and BC becomes more concentrated near the surface (Clarke and
82 Noone, 1985). This solar radiation reflecting capacity of snow insulates the sea ice, maintains
83 cold temperatures and delays ice melt in summertime. After the snow begins to melt and
84 because shallow melt ponds have an albedo of approximately 0.2 to 0.4, the surface albedo
85 drops to about 0.75 or even lower (0.15) as melt ponds grow and deepen (Singh and
86 Haritashya, 2011). These changes have been found to be important for the global energy

87 balance (Flanner et al., 2007; Hansen and Nazarenko, 2004) and, if enhanced by BC,
88 contribute to climate warming (Warren and Wiscombe, 1980).

89 Although BC in Arctic snow and ice has been found to be important for the Earth's
90 climate (Flanner et al., 2007; Sand et al., 2015), its large-scale temporal and spatial
91 distributions and exact origin are still poorly quantified (AMAP, 2015). Efforts to determine
92 the concentrations of BC in snow across the Arctic were made by Clarke and Noone (1985),
93 Doherty et al. (2010, 2013), Forsström et al. (2013), Ingvander et al. (2013) and McConnell et
94 al. (2007). This paper presents measurements of Elemental Carbon (EC) concentrations in
95 snow samples collected in spring 2014, 2015 and 2016 in the Kindo Peninsula (White Sea,
96 Karelia), around Arkhangelsk in northwestern European Russia, and in Western Siberia. In
97 the latter area, gas flaring emissions are very important. Flaring emissions are highly
98 uncertain because both activity data and emission factors are largely lacking. According to the
99 Global Gas Flaring Reduction Partnership (GGFR)
100 (<http://www.worldbank.org/en/programs/gasflaringreduction>), nearly 50 billion m³ of gas are
101 flared in Russia annually. The Russian flaring emissions in the Nenets/Komi regions and in
102 Khanty-Mansiysk are the major sources in Western Siberia and northwestern European
103 Russia. It has been reported that gas flaring in Russia contributes about 42% to the annual
104 average BC surface concentrations in the Arctic (Stohl et al., 2013).

105 The use of the terms EC and BC has been the topic of several scientific papers (for
106 example, Andreae and Gelencsér, 2006; Bond et al., 2013; Petzold et al., 2013). Petzold et al.
107 (2013) defined BC as a substance with 5 properties (see Table 1 in Petzold et al., 2013), for
108 which no single measurement instrument exists that is sensitive to all of them at the same
109 time. Consequently, BC cannot uniquely be measured, although some of its properties can,
110 such as the absorption coefficient σ_{ap} and the elemental carbon (EC) concentration, both
111 commonly measured in atmospheric monitoring networks across the world. Hence, the term
112 BC should be used qualitatively.

113 In the present study, EC concentrations on ice from three campaigns measured with
114 Thermal–Optical Analysis (TOA) (see section 2.2) are compared to simulation results from
115 the Lagrangian particle dispersion model (LPDM) FLEXPART. The model is used here for
116 the first time to quantify the sources contributing to BC in snow in Russia adopting a special
117 feature that was developed recently.

118 **2 Methodology**

119 **2.1 Collection and storage of snow samples**

120 Fresh snow samples were collected along a north–south transect between Tomsk and
121 the Yamal coast in February–March 2014 (23 samples), while in March 2015 sample
122 collection took place in the Kindo Peninsula and near the port of Arkhangelsk in the White
123 Sea (11 samples, Figure 1). Finally, in February–May 2016 samples were collected in the
124 Kindo Peninsula, in Arkhangelsk and between Tomsk and Yamal (20 samples). These areas
125 have been reported to receive pollution both from urban and gas flaring sources (Stohl et al.,
126 2013). For example, the gas flaring sources located in Yamal and Khanty-Mansiysk (Russia)
127 are in the main pathway along which sub-Arctic air masses travel to the Arctic (Stohl et al.,
128 2006). All sampling points were located more than 500 m away from roads to minimize the
129 direct influence from local traffic emissions. Information about sample collection such as the
130 location of sampling, the amount of snow collected and the depth at which snow was sampled
131 is reported in Table S1 and the sample locations are plotted in Figure 1.

132 Sampling was performed using a metal-free technique using pre-cleaned plastic shovels
133 and single-use vinyl gloves. Samples were stored in polyethylene bags which had been
134 thoroughly washed with 1 M HCl and rinsed with abundant deionised ultrapure water in the
135 laboratory prior to their use. After returning the samples to the laboratory, the snow was
136 allowed to melt at ambient temperature (18–20°C), and immediately filtered through quartz
137 47 mm fibre filters (2500QAT-UP Pall for samples collected in 2014 and QM-A Whatman for
138 samples collected in 2015 and 2016). The filters were dried at 60–70°C, wrapped in
139 aluminum foil and stored in a refrigerator. Quartz fiber filter collection efficiency of BC in
140 liquid samples can be less than 100% (Hadley et al., 2010; Ogren et al., 1983). To what extent
141 this has affected the levels reported in the present study is unknown. Thus the results
142 presented should be regarded as conservative estimates based on the assumption that some
143 BC might have been lost during filtration.

144 **2.2 Elemental Carbon measurements by Thermal–Optical Analysis (TOA)**

145 Elemental carbon (EC) content of the filters was measured at NILU's laboratories by thermal-
146 optical analysis (TOA), using the Sunset laboratory OC/EC instrument operated according to
147 the EUSAAR-2 protocol (Cavalli et al., 2010). A 1.5 cm² punch was cut from the filtered
148 snow samples for the analysis. Transmission was used for organic carbon (OC) charring
149 correction. Performance of the OC/EC instrument's is regularly intercompared as part of the

150 joint European Monitoring and Evaluation Programme (EMEP) Aerosols, Clouds, and Trace
151 gases Research InfraStructure Network (ACTRIS) quality assurance and quality control effort
152 (Cavalli et al., 2015).

153 **2.3 Measurements of carbonate (CO_3^{2-})-carbon by Thermal-Optical Analysis** 154 **(TOA) following thermal-oxidative pre-treatment**

155 The content of carbonate (CO_3^{2-})-carbon on the filters was measured by TOA,
156 following thermal-oxidative pretreatment based on the approach described by Jankowski et al.
157 (2008). A punch of 1.5 cm² from each filter was heated at 450 °C for 2 hours in ambient air to
158 remove OC and EC, but not CO_3^{2-} -carbon. The filter punch was subjected to TOA
159 immediately (30 sec) after thermal-oxidative pre-treatment. The split time (between OC and
160 EC) obtained for each filter punch used to determine the filter samples' content of EC (section
161 2.2) was also used to apportion CO_3^{2-} -carbon to OC and/or EC. The influence of CO_3^{2-} -
162 carbon evolving as EC, was accounted for by the following equation:

$$EC_{CO_3^{2-}}^{corr} = EC - EC_{CO_3^{2-}}$$

163 where $EC_{CO_3^{2-}}^{corr}$ is elemental carbon corrected for CO_3^{2-} -carbon that evolved as EC during
164 TOA, EC is elemental carbon and $EC_{CO_3^{2-}}$ is CO_3^{2-} -carbon that evolved as EC during TOA.
165 Applying this correction, EC values were 5-22% lower (see Supplementary Information).

166 **2.4 Emissions and modelling of black carbon**

167 The concentrations of BC in snow were simulated with the LPDM FLEXPART version
168 10 (Stohl et al., 1998, 2005). The model was driven with operational meteorological wind
169 fields retrieved from the European Centre for Medium-Range Weather Forecasts (ECMWF)
170 of 3-hour (for the years 2014 and 2015) and hour (for the year 2016) temporal resolution. The
171 ECMWF data have 137 vertical levels and a horizontal resolution of 1°×1° for the 2014 and
172 2015 simulations and 0.5°×0.5° for the 2016.

173 The simulations were conducted in backwards time (“retroplume”) mode, using a new
174 feature of FLEXPART to reconstruct wet and dry deposition with backward simulations
175 (Eckhardt et al., 2017). This new feature is an extension of the traditional possibility to
176 simulate atmospheric concentrations backward in time (Seibert and Frank, 2004; Stohl et al.,
177 2003). It is computationally efficient because it requires only two single tracer transport
178 simulations (one for wet deposition, one for dry deposition) for each measurement sample. To

179 reconstruct wet deposition amounts of BC, computational particles were released at altitudes
180 of 0 to 20 km at the locations where snow samples were taken, whereas to reconstruct dry
181 deposition, particles were released between the surface and 30 m at these locations. All
182 released particles represent a unity deposition amount, which was converted immediately (i.e.,
183 upon release of a particle) to atmospheric concentrations using the deposition intensity as
184 characterized either by dry deposition velocity or scavenging rate (for further details, see
185 Eckhardt et al., 2017). The concentrations were subsequently treated as in normal
186 “concentration mode” backward tracking (Seibert and Frank, 2004) to establish source-
187 receptor relationships between the emissions and deposition amounts. The termination time of
188 the particle release was the time at which the snow sample was collected, whereas the
189 beginning time was set as the time when the ECMWF precipitation at the sampling site,
190 accumulated backward in time, was equal to the water equivalent of the snow sample, up to
191 the specified sampling depth.

192 The model output consists of a spatially gridded sensitivity of the BC deposition at the
193 sampling location (receptor) to the BC emissions, equivalent to the backwards time mode
194 output for concentrations (Seibert and Frank, 2004; Stohl et al., 2003). BC deposition at the
195 snow sampling point can be computed (in mass per unit area) by multiplying the emission
196 sensitivity in the lowest model layer (the footprint emission sensitivity) with gridded
197 emissions from a BC emission inventory and integrating over the grid. The deposited BC can
198 be easily converted to BC snow concentration by taking into account the water equivalent
199 depth of the snow from ECMWF (in mm). In the present study, the ECLIPSE (Evaluating the
200 CLimate and Air Quality ImPacts of ShortlivEd Pollutants) version 5 emission inventory
201 (Klimont et al., 2016; Stohl et al., 2015) was used
202 (http://www.iiasa.ac.at/web/home/research/researchPrograms/air/Global_emissions.html).
203 The total emissions of BC from ECLIPSE in the areas of study are shown in Figure 1 (left
204 panel).

205 BC was assumed to have a density of 2 g m^{-3} in our simulations and a logarithmic size
206 distribution with an aerodynamic mean diameter of $0.25 \text{ }\mu\text{m}$ and a logarithmic standard
207 deviation of 0.3. Each computational particle released in FLEXPART represents an aerosol
208 population with a lognormal size distribution (see Stohl et al., 2005). Assumed aerodynamic
209 mean diameter and logarithmic standard deviation are used by FLEXPART’s dry deposition
210 scheme, which is based on the resistance analogy (Slinn 1982), and they are consistent with
211 those used in other transport models (see Evangeliou et al., 2016; Shiraiwa et al., 2008).

212 Below-cloud scavenging was determined based on the precipitation rate taken from ECMWF.
213 The in-cloud scavenging was based on cloud liquid water and ice content, precipitation rate
214 and cloud depth from ECMWF (Grythe et al., 2017). The FLEXPART user manual (available
215 from <http://www.flexpart.eu>) provides more information. All modelling results for this
216 sampling campaign can be viewed interactively at the URL
217 http://niflheim.nilu.no/NikolaosPY/SnowBC_141516.py.

218 **3 Results**

219 **3.1 Elemental Carbon concentrations measured in snow**

220 The spatial distribution of EC measured in snow samples from northwestern European
221 Russia and Western Siberia is shown in Figure 1(c) for each of the campaigns (2014, 2015
222 and 2016). There was large spatial variability in the distribution of EC in snow in 2014
223 ranging from 3 to 219 ng g⁻¹, with a median (\pm standard deviation) of 23 \pm 50 ng g⁻¹. The
224 highest EC concentrations in 2014 were observed in Western Siberia near Tomsk (147 to 219
225 ng g⁻¹). FLEXPART emission sensitivities for these samples showed that the air was coming
226 from the north and the east (see in http://niflheim.nilu.no/NikolaosPY/SnowBC_141516.py).
227 This explains the high concentrations of EC, as most of the anthropogenic BC sources are
228 located in these regions. In the rest of the snow samples for 2014, EC concentrations between
229 4 and 170 ng g⁻¹ were observed. High concentrations were observed near the Ob River
230 coinciding with air masses arriving mainly from Europe. During the 2015 field campaign, EC
231 concentrations were the highest near Arkhangelsk (175 ng g⁻¹), for which FLEXPART
232 showed that the air was coming from nearby areas
233 (http://niflheim.nilu.no/NikolaosPY/SnowBC_141516.py). Therefore, it is likely that the
234 samples were affected by direct emissions from the city or the port of Arkhangelsk. During
235 the same campaign, snow samples collected in the Kindo peninsula (on the White Sea coast)
236 showed high variability in EC concentrations (range: 46 – 152 ng g⁻¹, median=70 \pm 37 ng g⁻¹).
237 According to FLEXPART emission sensitivities, air masses were transported to Kindo
238 peninsula from central and southern Europe driven by an anticyclone over Scandinavia
239 (http://niflheim.nilu.no/NikolaosPY/SnowBC_141516.py). Finally, for the snow samples
240 collected outside Arkhangelsk, at the Kindo peninsula, and close to the Yamal Peninsula in
241 Western Siberia in 2016, EC concentrations ranged between 7–161 ng g⁻¹ (median: 40 \pm 39 ng
242 g⁻¹). Outside Arkhangelsk, EC concentrations varied widely from 31 to 161 ng g⁻¹ with a
243 median concentration in this region of 61 \pm 45 ng g⁻¹. This is far below the 175 ng g⁻¹ observed

244 in 2015, although there was only one sample collected in that year. In the Kindo Peninsula,
 245 EC was relatively constant in 2016 ranging between 25 and 35 ng g⁻¹ (median = 28±4 ng g⁻¹),
 246 which is more than 60% lower compared with the 2015 values (median = 70±37 ng g⁻¹).
 247 Finally, between Tomsk and Yamal, EC concentration was highly variable (7 – 119 ng g⁻¹)
 248 due to the different EC sources affecting snow (median = 50±38 ng g⁻¹). For instance, it is
 249 expected that gas flaring affects snow close to Yamal, while snow collected in the south
 250 (Tomsk) is likely influenced by sources in Europe or local urban emissions. Nevertheless, the
 251 highest concentrations (>100 ng g⁻¹) were observed north of 68°N, in the Yamal Peninsula.

252 We compared the measured EC concentrations in the snow samples with those
 253 calculated by FLEXPART. For this, the emission sensitivities were multiplied with the total
 254 emission fluxes from ECLIPSE (section 2.4). A scatter plot of modelled and measured snow
 255 concentrations is presented in Figure 1 (b). The results show a good correlation between
 256 modelled BC and measured EC concentrations for the 2015 and 2016 campaigns ($R_{2015} =$
 257 0.83 and $R_{2016} = 0.68$, $p - value < 0.05$), but weaker correlation for 2014 ($R_{2014} = 0.53$,
 258 $p - value < 0.05$). For further validation, the fractional bias (FB) of each individual sample
 259 was calculated together with the mean fractional bias (MFB) for observed EC and modelled
 260 BC for the 2014, 2015 and 2016 sampling campaigns as follows:

$$FB = \frac{C_m - C_o}{(C_m + C_o)/2} \times 100\% \text{ and } MFB = \frac{1}{N} \sum_{i=1}^N \frac{C_m - C_o}{(C_m + C_o)/2} \times 100\%$$

261 where C_m and C_o are the modelled BC and measured EC concentrations and N is the total
 262 number of observations for each year. The FB for individual samples is shown in Figure S 1.
 263 FB is a useful model performance indicator because it is symmetric and gives equal weight to
 264 underestimations and overestimations (it takes values between -200% and 200%). It is used
 265 here to show the locations where modelled BC concentrations in snow over- or underestimate
 266 observations (see Figure S 1). The MFB of the model for the 2014 snow measurements was -
 267 42%, which shows that the model underestimated observations. In total, the model
 268 underestimated concentrations for 17 out of 23 samples with FB values ranging from -168%
 269 to -30%, whereas for the rest (six samples) FB values ranged between 20% and 148%
 270 (median: -56%±81%) (Figure S 1). In 2015, the MFB of the model was -48% (median: -
 271 56%±32%), where 11 out of 12 values were underestimated by the model showing FB values
 272 that ranged between -101% and -7% (one FB value was found to be 12%). For 2016, FB
 273 values of the simulated concentrations of BC in snow show another set of underestimation

274 (median: $-13\% \pm 73\%$) varying from -198% to -0.3% for 12 out of 19 samples. For the
275 remaining seven samples, the model predicted higher concentrations compared with
276 observations (10% to 75%) (Figure S 1). The root mean square error (RMSE) was computed,
277 which is frequently used to measure differences between values predicted by a model and the
278 values actually observed. RMSE values were estimated to be quite high, between 37 and 49
279 ng g^{-1} , due to the large variation of the observed EC concentrations.

280 The levels of EC in snow presented here are relatively high compared to previously
281 reported concentrations in the Arctic. Apart from Aamaas et al. (2011) who measured
282 maximum EC concentration in snow close to the airport of Svalbard of more than 1000 ng g^{-1} ,
283 most of the reported levels of EC in the relevant literature are close to our findings. For
284 instance, Ruppel et al. (2014) found that EC concentrations have been increasing up to 103 ng
285 g^{-1} since 1970 in Svalbard. McConnell et al. (2007) reported that the BC concentrations
286 measured at the D4 ice-core site in Greenland were 10 ng g^{-1} , at maximum, which most likely
287 originated from biomass burning in the conifer-rich boreal forest of the Eastern and Northern
288 United States and Canada. Forsström et al. (2013) reported concentrations as high as 88 ng g^{-1}
289 in Scandinavia, and lower ones at higher latitudes ($11\text{--}14 \text{ ng g}^{-1}$ in Svalbard, $7\text{--}42 \text{ ng g}^{-1}$ in
290 the Fram Strait, and 9 ng g^{-1} in Barrow). Svensson et al. (2013) collected snow samples from
291 Tyresta National Park and Pallas-Yllästunturi National Park in Sweden. Tyresta is a relatively
292 polluted site located circa 25 km from the city centre of Stockholm with a population of about
293 2 million people. Yllästunturi National Park is located in Arctic Finland and a clean site with
294 no major city influencing the local and regional air. The concentration of EC in Pallas-
295 Yllästunturi was between 0 and 140 ng g^{-1} , while in Tyresta the BC concentrations were up to
296 more than 7 times higher ($53\text{--}810 \text{ ng g}^{-1}$). Furthermore, Doherty et al. (2010) in the most
297 complete dataset for the Arctic snow and ice BC reported highly variable concentrations (up
298 to 800 ng g^{-1}) for five consecutive years (2005–2009). Finally, in the most recent dataset for
299 snow BC, Macdonald et al. (2017) reported BC concentrations ranging from 0.3 to 15 ng g^{-1}
300 were reported for the samples collected near the Alert observatory (see section 4.1).

301 **3.2 Sources and origin of BC**

302 We further analysed the model output in order to calculate relevant contributions from
303 various BC source types to BC concentrations in snow (for method description, see section
304 2.4). ECLIPSE emissions include waste burning (WST), industrial combustion and processing
305 (IND), surface transportation (TRA), power plants, energy conversion, and extraction (ENE),

306 residential and commercial combustion (DOM), gas flaring (FLR), while biomass burning
307 (BB) emissions were adopted from the Global Fire Emissions Database, Version 4
308 (GFEDv4.1) (Giglio et al., 2013). The results are depicted in Figure 2 for the sampling
309 campaigns of 2014, 2015 and 2016 in Western Siberia and North-Western European Russia,
310 sorted from the northernmost to the southernmost sampling location.

311 In 2014, TRA contributed about 18%, on average, to the simulated BC in snow, DOM
312 28%, FLR 44%, whereas ENE and IND were less significant. Maxima of TRA, DOM, and
313 FLR contributions were observed at a latitude of about 65°N, where measured EC and
314 modelled BC were similar. An example of the contribution from the aforementioned
315 dominant sources to snow BC concentrations for the highest measured EC concentration in
316 snow is shown in Figure 3. The transport sector includes emissions from all land-based
317 transport of goods, animals and persons. It is more significant in southern Russia and close to
318 the borders with Kazakhstan and Mongolia, where a large number of major Russian cities
319 (e.g., Moscow, Kazan, Samara, Yekaterinburg, Tomsk, Novosibirsk, Krasnoyarsk, etc...) are
320 located and connected with each other by federal highways. Residential and commercial
321 combustion includes emissions from combustion in households and public and commercial
322 buildings. Therefore, it is expected to be high for areas that consist of large population centres
323 (Figure 3). FLR emissions were found to contribute the most in this example with a total
324 concentration from this sector of 19.7 ng g⁻¹ (compared with 12.6 and 16.5 ng g⁻¹ in TRA and
325 DOM, respectively) (Figure 3).

326 In the Kindo Peninsula and in Arkhangelsk, where snow sampling took place in 2015,
327 the main contributions to snow BC were from DOM (47%), TRA (30%), BB (7%), and FLR
328 (6%) (see Figure 2). Similar to EC measurements in snow, simulated BC was also higher than
329 in 2014, as the sampling sites were located closer to strong sources in Europe (Kindo) and
330 close to a populated area (Arkhangelsk) with a strong regional impact. The highest
331 concentration of EC was observed in the Kindo Peninsula (33.13°E – 66.53°N). Figure 4
332 shows the spatial distribution of emissions that contributed to simulated snow BC at the
333 sampling point where the highest BC concentration was observed. In this case, TRA and
334 DOM emissions from Europe mostly affected snow in the Kindo Peninsula whereas FLR
335 emissions were very low due to the long distance from the sampling point. Emissions from an
336 unusual late winter/early spring episode of BB in the borders of Belarus, Ukraine and Russia
337 also affected BC concentrations in snow in northwestern European Russia (Figure 4). The
338 importance of episodic BB releases in Russia, the miscalculation of satellite retrieved BB

339 emissions and their impact in Arctic concentrations in early spring has been explained by
340 Evangeliou et al. (2016) and Hao et al. (2016). BB emissions, originating mostly from Eastern
341 Europe, contributed about 19.4 ng g^{-1} to the snow concentration at the receptor point (Figure
342 4). TRA and DOM emissions were the dominant sources for this sampling point, contributing
343 33.6 and 47.2 ng g^{-1} , respectively (Figure 4).

344 Finally, in 2016, when samples were collected at the Kindo Peninsula, in Arkhangelsk
345 and in Yamal, DOM, FLR and TRA contributed, on average, 31%, 29% and 27%,
346 respectively (see Figure 2 (c)). Similar to the measured EC concentrations in snow, simulated
347 concentrations of BC in 2016 were lower than those in 2015, on average. The highest
348 measured EC concentration was observed in the Khanty-Mansiysk region ($72.94^{\circ}\text{E} -$
349 65.36°N), which mirrors the simulated BC concentration at the same point very well. The
350 much higher contribution from TRA at this sampling point (38.6 ng g^{-1}) (Figure 5 (b)) is
351 attributed to emissions from Southern Russia (e.g., Tomsk), where all the main cities in
352 Russia are located. Another large fraction of TRA emissions comes from Central and Eastern
353 Europe (see also in http://niflheim.nilu.no/NikolaosPY/SnowBC_141516.py). Similar to
354 TRA, emissions from DOM were mostly transported to Khanty-Mansiysk from Central and
355 Eastern Europe, as well as from Turkey contributing 36.6 ng g^{-1} (Figure 5). As previously
356 mentioned, the sampling point where the highest EC concentration was measured is located
357 inside the largest gas flaring region of Russia. In addition, the corresponding emission
358 sensitivity maps showed that the air was coming from south passing directly through this high
359 emission region making FLR emissions the highest contributing source (88.8 ng g^{-1}) (Figure
360 5).

361 **4 Discussion**

362 **4.1 Cross validation of modelled BC concentrations with public datasets**

363 In this section, we present an effort to further validate our model calculations of BC
364 concentrations in snow. For this purpose, BC concentrations in snow that were adopted from
365 Doherty et al. (2010) were compared with modelled BC concentrations in snow that were
366 simulated with FLEXPART as described in section 2.4. Samples were collected in Alaska,
367 Canada, Greenland, Svalbard, Norway, Russia, and the Arctic Ocean during 2005–2009, on
368 tundra, glaciers, ice caps, sea ice, frozen lakes, and in boreal forests. Snow was collected
369 mostly in spring, when the combination of snow cover and exposure to sunlight is at
370 maximum and before the snow had started to melt. Samples of melting snow collected in the

371 summer of 2008 from Greenland and from Tromsø, Norway, were removed from the study, as
372 we have no knowledge about the depth of the melt layer and effects of the percolation of
373 meltwater through the snowpack. All samples were collected away from local sources of
374 pollution. In many locations (Canadian Arctic, Russia, Greenland, Tromsø and Ny-Ålesund)
375 samples were gathered at different depths throughout the snowpack, giving information on the
376 seasonal evolution of BC concentrations as the snow accumulated (and/or sublimated)
377 throughout the winter. In these cases only the surface BC was taken into account. The snow
378 was melted and filtered, and the filters were analysed in a specially designed
379 spectrophotometer system to infer the concentration of BC (for more information see Doherty
380 et al., 2010). In contrast to our findings for the origin of snow BC in the Russian Arctic, a
381 source apportionment analysis performed in the 2008 and 2009 measurements (Hegg et al.,
382 2010) from this dataset showed that the dominant source of BC in the Arctic snow pack was
383 biomass burning. Specifically in Eastern Siberia biomass burning of crops and grasslands
384 contributed more snow BC in high latitudes than boreal forest fires, in contrast to the
385 Canadian Arctic.

386 A comparison of modelled (FLEXPART) and measured BC concentrations (Doherty et
387 al., 2010) in snow is depicted in Figure S 2. The model captures snow BC concentrations
388 relatively well in most of the Arctic regions except for the Canadian Arctic, where the
389 modelled concentrations of snow in 2007 were significantly higher. Samples from the same
390 region in other years showed moderate agreement with modelled values. Similar to our
391 finding for the new Russian measurements, the model output, with a MFB of -51%, tends to
392 underestimate deposition. The RMSE was estimated to be 52 ng g^{-1} , which is acceptable
393 considering that the variation of snow concentrations in the dataset ranged from 0.3 to 783 ng
394 g^{-1} . The highest measured concentrations of snow BC were observed in Russia, where the
395 model showed a good spatial agreement. For instance, the highest values were obtained in
396 Western Siberia, close to the gas flaring regions of the Nenets/Komi oblast, as well as in
397 southeastern and northeastern Russia, where air masses were arriving from high emitting
398 sources in southeastern Asia. Lower biases in modelled BC concentrations were observed in
399 northern Siberia with the exception of a few samples at the coasts of the Kara Sea and
400 northeastern Siberia. Furthermore, biased BC concentrations were also observed in Greenland
401 and northern Canada. In Western Siberia, BC in snow presented in Doherty et al. (2010)
402 between 2005–2009 was $101 \pm 153 \text{ ng g}^{-1}$ on average, which is very close to the average value
403 of measured EC obtained from the sampling 2014–2016 campaigns ($83 \pm 37 \text{ ng g}^{-1}$).

404 From total number of samples presented in (Doherty et al., 2010) that were used here
405 for validation, only six were collected in the Yamal Peninsula similar as part of the data
406 presented in the current paper. The rest was collected in Nenets/Komi region and in Eastern
407 Russia and cannot be directly compared with snow EC measurements from the 2014 – 2016
408 campaigns. BC concentrations in Yamal Peninsula in 2007 ranged from 4.1 to 17.6 ng g⁻¹
409 (Average±SD: 10.1±4.8 ng g⁻¹). In the same region, we report EC concentrations to be more
410 than double varying between 6.6 to 55 ng g⁻¹ (Average±SD: 25.7±15.8 ng g⁻¹), whereas there
411 were two samples that showed EC concentrations of more than 100 ng g⁻¹. As mentioned in
412 section 2.1 the sampling of snow for the EC analysis took place more than 500 m away from
413 roads to minimize influence from traffic emissions, while a similar statement is also found in
414 the (Doherty et al., 2010) data. Nevertheless, considering that the samples were not collected
415 from the same regions exactly and at the same time, no safe conclusions can be obtained.

416 Modelled BC concentrations simulated with FLEXPART were also compared with
417 snow BC concentrations from samples collected at the Global Atmosphere Watch
418 Observatory at Alert, Nunavut, from September 14th, 2014 to June 1st, 2015 and they are
419 available in Macdonald et al. (2016). Alert is a remote outpost in the Canadian high Arctic, at
420 the northern coast of Ellesmere Island (82°27' N, 62°30' W), with a small transient
421 population of research and military personnel. Sampling details and analytical methodologies
422 used for the analysis of BC can be found in Macdonald et al. (2016). BC concentrations in
423 FLEXPART were simulated as in all previous analyses described in this paper (see section
424 2.4.). Timeseries of simulated and measured BC are depicted in Figure S 3 for the whole
425 sampling period. As before, a correlation coefficient (*R*) of 0.63 indicates that our model
426 captures the temporal variation of the measured BC in snow. The RMSE was estimated to be
427 almost 63 ng g⁻¹, a relatively high value. The MFB of 47% indicates a strong overestimation
428 of snow concentrations, although in many samples the opposite was also observed (Figure S
429 3). This is in contrast to the previous data sets discussed, for which the model underestimated
430 measurements.

431 Further analysis was carried out to adequately understand the origin of the
432 aforementioned overestimations in the Canadian Arctic in both datasets (Doherty et al., 2010;
433 Macdonald et al., 2017), as they are shown to be rather systematic. For this reason, we have
434 calculated the average footprint emission sensitivities and the average BC contribution from
435 the major sources in ECLIPSE for the 2007 snow samples in the Canada Arctic and for Alert
436 samples. We have chosen these samples, because they were three or more times higher than

437 the observations and in this way we can locate the observed overestimations predicted with
438 FLEXPART (Figure 6).

439 Regarding the model overestimation for the 2007 samples, the average footprint
440 emission sensitivity showed that the air was coming from continental regions of Canada with
441 a smaller contribution from Scandinavia (Figure 6). The highest emission sources for these
442 samples were TRA and DOM that contributed almost 80% to the snow concentrations,
443 whereas forest fires were less important at the time of sampling. Two hot spots were
444 identified, one along the borders of Canada with USA and another, of smaller intensity, in
445 southeastern Asia. A similar emission sensitivity was obtained for the same area of the
446 Canadian Arctic in 2009 only slightly shifted to the north; simulated concentrations were in
447 very good agreement with observations (Figure S 2). This shows that the model
448 overestimation for the 2007 samples is likely attributed to an overestimation of TRA and
449 DOM sources in North America in ECLIPSE for 2007. For the Alert samples, for which the
450 model strongly overestimated BC, the major sources were TRA and FLR, which contributed
451 55%, and BB which contributed about 7 ng g^{-1} (22%) on average (Figure 6). Anthropogenic
452 BC arriving from Europe and Russia has been previously shown to be important for Alert air
453 pollutant concentrations (Sharma et al., 2013). The model overestimation of BC in snow
454 samples at Alert needs further investigation. It is likely that it originates from anthropogenic
455 emissions in northwestern America or in Europe, because forest fires in Canada and Russia,
456 although important for Alert (e.g., Qi et al., 2017), were not significant in the present
457 comparison.

458 **4.2 Model deviation from snow EC measurements and region-specific** 459 **contribution of sources**

460 It has been shown that measured concentrations of EC in snow in northwestern
461 European Russia and Western Siberia were underestimated in FLEXPART (Figure 2). This
462 was confirmed by the calculated fractional bias (see section 3.2), the spatial distribution of
463 which is shown in Figure S 1. To examine whether this underestimation was due to missing
464 emission sources or errors in modelled transport and deposition, we have calculated the
465 average footprint emission sensitivity for those sampling points, for which FLEXPART
466 strongly ($FB < -100\%$) and slightly ($-100\% < FB < 0\%$) underestimated the observed
467 values. The average footprint emission sensitivities are shown in Figure 7 together with the
468 locations of active fires in the last two months before the sample collection. The fire data

469 were adopted from MODIS (Moderate Resolution Imaging Spectroradiometer) (Giglio et al.,
470 2003) and the gas flaring facilities from the Global Gas Flaring Reduction Partnership
471 (GGFR) (<http://www.worldbank.org/en/programs/gasflaringreduction>).

472 When the model strongly underestimated the measured EC ($FB < -100\%$), the
473 average footprint emission sensitivity showed the highest values over the Yamal Peninsula
474 and the agglomeration of many gas flares in Khanty-Mansiysk (Figure 7 (b)). This might
475 confirm the finding of Huang et al. (2014) that gas flaring emissions in the ECLIPSE
476 inventory, while very high, are still underestimated. According to a related study by Huang
477 and Fu (2016), Russia contributes 57% to the global BC emissions from gas flaring.
478 Underestimation of modelled atmospheric concentrations compared to observations from the
479 Barents and Kara Seas was recently also reported by Popovicheva et al. (2017), although the
480 underestimation was relatively small.

481 When FLEXPART showed a moderate underestimation of EC concentrations in snow
482 ($-100\% < FB < 0\%$), the emission sensitivity was high near Arkhangelsk and over
483 Scandinavia (Figure 7). BC emissions in Scandinavia are considered relatively low in most
484 inventories and contribute no more than 6.5% to the global emissions in ACCMIP (Aerosol
485 Chemistry Climate Model Intercomparison Project) (Lamarque et al., 2013), 6.2% in
486 EDGARv4.2 (Emission Database for Global Atmospheric Research) (Olivier et al., 2005),
487 2.1% in MACCity (Monitoring Atmospheric Composition & Climate / megaCITY - Zoom for
488 the ENvironment) (Hollingsworth et al., 2008; Stein et al., 2012) and 3.3% in ECLIPSE
489 (Klimont et al., 2016). The highest emission sensitivity was found over northwestern Russia
490 (Figure 7), a region which includes Murmansk. Pollution levels in Murmansk could be high
491 due to emissions from local industry, mining, heating and transport (Law and Stohl, 2007).
492 Another potential source region was Nenets/Komi area and Western Kazakhstan, where a few
493 other flaring facilities are located (Figure 7).

494 Figure 7 shows that the underestimation of observed EC concentrations in snow
495 strongly depends on the region, where samples are collected. In Western Siberia, the
496 underestimation was larger than in northwestern European Russia. For this reason, we have
497 computed the average region-specific emission sensitivities and the average region-specific
498 contribution from the major polluting sources identified in ECLIPSE dataset. We distinguish
499 between three regions, northwestern European Russia, Western Siberia (north of 62 °N) and
500 Western Siberia (south of 62 °N) (Figure S 4 – S 6). For the samples collected in northwestern

501 European Russia (Figure S 4), an average contribution of 21.6 ng g⁻¹ from all sources was
502 estimated to have originated mainly from TRA (7.7 ng g⁻¹) and DOM (10.4 ng g⁻¹) sources in
503 Finland. The contribution from BB and FLR emissions was insignificant (8% and 6%,
504 respectively), whereas the rest of the ECLIPSE sources were negligible (IND, ENE, WST).
505 For the samples collected at high latitudes in Western Siberia, the average contribution from
506 all sources was more than 4 times higher (86 ng g⁻¹) than those observed in northwestern
507 European Russia (Figure S 5). FLR emissions accounted for 40% of the total contribution,
508 which reflect the proximity of the sampling site to the main flaring facilities of Russia. The
509 average contribution from TRA activities in Europe and southeastern Russia to the northern
510 part of Western Siberia was 24%. Finally, DOM emissions in Eastern Europe also contributed
511 another 28%. Finally, for the samples that were collected in the southern part of the Western
512 Siberia an average contribution of 47.4 ng g⁻¹ was estimated from all sources included in
513 ECLIPSE (Figure S 6). The highest contributing categories were TRA and DOM, whereas
514 FLR appeared to contribute less, although the sampling site is close to Khanty-Mansiysk
515 flaring region. This is attributed to the prevailing winds that forced flaring emissions to a
516 northernmost direction opposite to the location of the sampling stations (see Figure S 6).

517 Overall, the region-specific analysis of the sources contributing to modelled BC in
518 snow showed that the DOM, FLR and/or TRA sources might explain the model
519 underestimation in high Arctic. However, in the most recent assessments of BC of the higher
520 Arctic (Popovicheva et al., 2017; Winiger et al., 2017), it was shown that ECLIPSE captures
521 levels of BC quite well, whereas FLR emissions might have a smaller impact in the Central
522 Siberian Arctic (Tiksi) than previously estimated. Surprisingly, the average contribution from
523 BB in lower latitudes was extremely low in all Western Siberia (Figure S 5 and S 6), despite
524 the fact that sampling took place in springtime, where BB becomes important. Evangelidou et
525 al. (2016) reported that using a different dataset, that is based on the same approach as GFED,
526 but includes updated emission factors for Eurasia, surface concentrations of BC in the Arctic
527 stations can be substantially higher. This shows the need for further investigation of BC
528 sources in the Russian Arctic.

529 **5 Conclusions**

530 We have analysed snow samples collected in Western Siberia and northwestern
531 European Russia in 2014, 2015 and 2016 with respect to EC. This region is of major interest
532 due to its large uncertainty in BC emissions and because it is located in the main transport

533 route of BC to the Arctic. An effort to constrain the sources that contribute to measured
534 concentration in BC in snow was made using the LPDM FLEXPART (version 10).

535 The observed EC levels in snow varied widely within and between regions (3–219 ng g⁻¹
536 for 2014, 46–175 ng g⁻¹ in 2015 and 7–161 ng g⁻¹ in 2016), and are in the upper range of
537 previously reported concentrations of EC and BC in snow in the Arctic region. However, the
538 observed levels presented here appear typical for Western Siberia, which is subject to high
539 domestic Russian emissions as well as to transport from distant European ones.

540 The snow BC concentrations predicted by the model are in a fair agreement with EC
541 observations over Western Siberia and northwestern European Russia ($R = 0.5 - 0.8$).
542 However, the calculated MFB values (-48% to -27%) showed that the model systematically
543 underestimated observations in Russia. This underestimation strongly depended on the region
544 where the samples were collected. In northwestern European Russia, the main contributing
545 sources were TRA and DOM mainly from adjacent regions in Finland. TRA and DOM
546 contributed double to snow BC sampled at low latitudes of Western Siberia (<60°N) as
547 compared to samples collected over regions above 60°N; the majority of these emissions
548 originating from highly populated centres in Central Europe. Finally, in higher latitudes of
549 Western Siberia (>60°N), snow BC concentrations were further increased mainly due to FLR
550 emissions from facilities located close to the snow sampling points.

551 The modelled BC concentrations in snow were further investigated using two
552 independent public measurement datasets that include samples from all over the Arctic for the
553 period 2005 to 2009 and from Alert in 2014 and 2015. The model captured levels of BC fairly
554 well despite the large variation in measured concentrations. An exception was observed in
555 North America in spring 2007 and in Alert observatory in late winter – early spring 2015. In
556 both cases, the major sources were along the Canadian borders with USA and in Western
557 Europe. Considering the fact that similar deviations were not observed in samples collected in
558 the area during other years, it is likely that some of the prevailing sources of BC in this region
559 show strong temporal variability in their emissions, and this is not taken into account in
560 ECLIPSE inventory. Previously reported average measurements of BC concentrations in
561 snow in Western Siberia and northwestern European Russia were 101 ± 153 ng g⁻¹, which is
562 about 20% higher than the EC measurements presented here (83 ± 37 ng g⁻¹).

563 **Data availability.** All data used for the present publication can be obtained from the
564 corresponding author upon request.

565 *Competing interests.* The authors declare that they have no conflict of interest.

566 *Acknowledgements.* We would like to acknowledge the project entitled “Emissions of
567 Short-Lived Climate Forcers near and in the Arctic (SLICFONIA)”, which was funded by the
568 NORRUSS research program of the Research Council of Norway (Project ID: 233642) and
569 the Russian Fund for Basic Research (project No. 15-05-08374) for funding snow sampling in
570 the White Sea catchment area. We also thank Sergey Belorukov, Andrey Boev, Anton
571 Bulokhov, Victor Drozdov, Sergey Kirpotin, Ivan Kritzkov, Rinat Manasypov, Ivan
572 Semenyuk, and Alexander Yakovlev for helping during the three expeditions and
573 Academician Alexander P. Lisitzin for his valuable recommendations. O. S. Pokrovsky and S.
574 N. Vorobiev acknowledge support from BIO-GEO-CLIM grant No 14.B25.31.0001 for
575 sampling in Western Siberia. Acknowledgements are also owed to IIASA (especially Chris
576 Heyes and Zig Klimont) for providing the BC emission dataset. Computational and storage
577 resources for the FLEXPART simulations have been provided by NOTUR (NN9419K) and
578 NORSTORE (NS9419K). All plots from FLEXPART simulations have been included in an
579 interactive website for fast visualization
580 (http://niflheim.nilu.no/NikolaosPY/SnowBC_141516.py). All results can be accessed upon
581 request to the corresponding author of this manuscript.

582 *Author Contributions.* N. Evangeliou designed and performed the modelling experiments
583 and wrote the paper. V. P. Shevchenko organised and performed the sampling of EC, K.-E.
584 Yttri performed all the TOA of the snow samples. S. Eckhardt modified FLEXPART model
585 for the calculation of footprint emission sensitivities for deposited mass. E. Sollum wrote an
586 algorithm that computes the starting date of the FLEXPART releases based on the water
587 equivalent volume from ECMWF. O. S. Pokrovsky, V. O. Kobelev, V. B. Korobov, A. A.
588 Lobanov, D. P. Starodymova and S. N. Vorobiev assisted the sampling campaigns in Western
589 Siberia and northwestern European Russia during 2014–2016. R. L. Thompson and A. Stohl
590 supervised the study and wrote parts of the paper.

591

592 **References**

593 Aamaas, B., Bøggild, C. E., Stordal, F., Berntsen, T., Holmén, K. and Ström, J.: Elemental
594 carbon deposition to Svalbard snow from Norwegian settlements and long-range transport,
595 Tellus, Ser. B Chem. Phys. Meteorol., 63(3), 340–351, doi:10.1111/j.1600-
596 0889.2011.00531.x, 2011.

597 AMAP: AMAP assessment 2015: Black carbon and ozone as Arctic climate forcers, Arctic
598 Monitoring and Assessment Programme (AMAP), Oslo, Norway., 2015.

599 Andreae, M. O. and Gelencsér, A.: Black carbon or brown carbon? The nature of light-
600 absorbing carbonaceous aerosols, *Atmos. Chem. Phys.*, 6(3), 3419–3463, doi:10.5194/acpd-6-
601 3419-2006, 2006.

602 Bond, T. C., Streets, D. G., Yarber, K. F., Nelson, S. M., Woo, J. H. and Klimont, Z.: A
603 technology-based global inventory of black and organic carbon emissions from combustion, *J.*
604 *Geophys. Res. D Atmos.*, 109(14), 1–43, doi:10.1029/2003JD003697, 2004.

605 Bond, T. C., Doherty, S. J., Fahey, D. W., Forster, P. M., Berntsen, T., Deangelo, B. J.,
606 Flanner, M. G., Ghan, S., Kärcher, B., Koch, D., Kinne, S., Kondo, Y., Quinn, P. K., Sarofim,
607 M. C., Schultz, M. G., Schulz, M., Venkataraman, C., Zhang, H., Zhang, S., Bellouin, N.,
608 Guttikunda, S. K., Hopke, P. K., Jacobson, M. Z., Kaiser, J. W., Klimont, Z., Lohmann, U.,
609 Schwarz, J. P., Shindell, D., Storelvmo, T., Warren, S. G. and Zender, C. S.: Bounding the
610 role of black carbon in the climate system: A scientific assessment, *J. Geophys. Res. Atmos.*,
611 118(11), 5380–5552, doi:10.1002/jgrd.50171, 2013.

612 Brandt, R. E., Warren, S. G., Worby, A. P. and Grenfell, T. C.: Surface albedo of the
613 Antarctic sea ice zone, *J. Clim.*, 18(17), 3606–3622, doi:10.1175/JCLI3489.1, 2005.

614 Cavalli, F., Viana, M., Yttri, K. E., Genberg, J. and Putaud, J.-P.: Toward a standardised
615 thermal-optical protocol for measuring atmospheric organic and elemental carbon: the
616 EUSAAR protocol, *Atmos. Meas. Tech.*, 3(1), 79–89, doi:10.5194/amt-3-79-2010, 2010.

617 Cavalli, F., Putaud, J.-P. and Yttri, K. E.: Availability and quality of the EC and OC
618 measurements within EMEP, including results of the fifth interlaboratory comparison of
619 analytical methods for carbonaceous particulate matter within EMEP (2012)., 2015.

620 Clarke, A. D. and Noone, K. J.: Soot in the arctic snowpack: a cause for perturbations in
621 radiative transfer, *Atmos. Environ.*, 41(SUPPL.), 64–72, doi:10.1016/0004-6981(85)90113-1,
622 1985.

623 Doherty, S. J., Warren, S. G., Grenfell, T. C., Clarke, A. D. and Brandt, R. E.: Light-
624 absorbing impurities in Arctic snow, *Atmos. Chem. Phys.*, 10(23), 11647–11680,
625 doi:10.5194/acp-10-11647-2010, 2010.

626 Doherty, S. J., Grenfell, T. C., Forsström, S., Hegg, D. L., Brandt, R. E. and Warren, S. G.:
627 Observed vertical redistribution of black carbon and other insoluble light-absorbing particles
628 in melting snow, *J. Geophys. Res. Atmos.*, 118(11), 5553–5569, doi:10.1002/jgrd.50235,
629 2013.

630 Eckhardt, S., Cassiani, M., Evangeliou, N., Sollum, E., Pisso, I. and Stohl, A.: Source-
631 receptor matrix calculation for deposited mass with the Lagrangian particle dispersion model
632 FLEXPART v10.2 in backward mode, *Geosci. Model Dev. Discuss.*, submitted, 2017.

633 Evangeliou, N., Balkanski, Y., Hao, W. M., Petkov, A., Silverstein, R. P., Corley, R.,
634 Nordgren, B. L., Urbanski, S. P., Eckhardt, S., Stohl, A., Tunved, P., Crepinsek, S., Jefferson,
635 A., Sharma, S., Nøjgaard, J. K. and Skov, H.: Wildfires in northern Eurasia affect the budget
636 of black carbon in the Arctic—a 12-year retrospective synopsis (2002–2013), *Atmos. Chem.*
637 *Phys.*, 16(12), 7587–7604, doi:10.5194/acp-16-7587-2016, 2016.

638 Flanner, M. G., Zender, C. S., Randerson, J. T. and Rasch, P. J.: Present-day climate forcing
639 and response from black carbon in snow, *J. Geophys. Res. Atmos.*, 112(11), 1–17,
640 doi:10.1029/2006JD008003, 2007.

641 Forsström, S., Isaksson, E., Skeie, R. B., Ström, J., Pedersen, C. A., Hudson, S. R., Berntsen,
642 T. K., Lihavainen, H., Godtliebsen, F. and Gerland, S.: Elemental carbon measurements in
643 European Arctic snow packs, *J. Geophys. Res. Atmos.*, 118(24), 13614–13627,
644 doi:10.1002/2013JD019886, 2013.

645 Forster, C., Wandinger, U., Wotawa, G., James, P., Mattis, I., Althausen, D., Simmonds, P.,
646 O’Doherty, S., Jennings, S. G., Kleefeld, C., Schneider, J., Trickl, T., Kreipl, S., Jäger, H. and
647 Stohl, A.: Transport of boreal forest fire emissions from Canada to Europe, *J. Geophys. Res.*,
648 106, 22887, doi:10.1029/2001JD900115, 2001.

649 Giglio, L., Descloitres, J., Justice, C. O. and Kaufman, Y. J.: An enhanced contextual fire
650 detection algorithm for MODIS, *Remote Sens. Environ.*, 87(2–3), 273–282,
651 doi:10.1016/S0034-4257(03)00184-6, 2003.

652 Giglio, L., Randerson, J. T. and van der Werf, G. R.: Analysis of daily, monthly, and annual
653 burned area using the fourth-generation global fire emissions database (GFED4), *J. Geophys.*
654 *Res. Biogeosciences*, 118, 317–328, doi:10.1002/jgrg.20042, 2013, 2013.

655 Grythe, H., Kristiansen, N. I., Groot Zwaaftink, C. D., Eckhardt, S., Ström, J., Tunved, P.,

656 Krejci, R. and Stohl, A.: A new aerosol wet removal scheme for the Lagrangian particle
657 model FLEXPARTv10, *Geosci. Model Dev.*, 10, 1447–1466, doi:10.5194/gmd-10-1447-
658 2017, 2017.

659 Hadley, O. L., Corrigan, C. E., Kirchstetter, T. W., Cliff, S. S. and Ramanathan, V.: Measured
660 black carbon deposition on the Sierra Nevada snow pack and implication for snow pack
661 retreat, *Atmos. Chem. Phys.*, 10(15), 7505–7513, doi:10.5194/acp-10-7505-2010, 2010.

662 Hansen, J. and Nazarenko, L.: Soot climate forcing via snow and ice albedos, *Proc. Natl.*
663 *Acad. Sci. U. S. A.*, 101(2), 423–428, doi:10.1073/pnas.2237157100, 2004.

664 Hao, W. M., Petkov, A., Nordgren, B. L., Silverstein, R. P., Corley, R. E., Urbanski, S. P.,
665 Evangeliou, N., Balkanski, Y. and Kinder, B.: Daily black carbon emissions from fires in
666 Northern Eurasia from 2002 to 2013, *Geosci. Model Dev. Discuss.*, (April), 1–24,
667 doi:10.5194/gmd-2016-89, 2016.

668 Hegg, D. A., Warren, S. G., Grenfell, T. C., Doherty, S. J., Larson, T. V. and Clarke, A. D.:
669 Source attribution of black carbon in arctic snow, *Environ. Sci. Technol.*, 43(11), 4016–4021,
670 doi:10.1021/es803623f, 2009.

671 Hegg, D. A., Warren, S. G., Grenfell, T. C., Doherty, S. J. and Clarke, A. D.: Sources of light-
672 absorbing aerosol in arctic snow and their seasonal variation, *Atmos. Chem. Phys.*, 10(22),
673 10923–10938, doi:10.5194/acp-10-10923-2010, 2010.

674 Hollingsworth, A., Engelen, R. J., Textor, C., Benedetti, A., Boucher, O., Chevallier, F.,
675 Dethof, A., Elbern, H., Eskes, H., Flemming, J., Granier, C., Kaiser, J. W., Morcrette, J. J.,
676 Rayner, P., Peuch, V. H., Rouil, L., Schultz, M. G. and Simmons, A. J.: Toward a monitoring
677 and forecasting system for atmospheric composition: The GEMS project, *Bull. Am. Meteorol.*
678 *Soc.*, 89(8), 1147–1164, doi:10.1175/2008BAMS2355.1, 2008.

679 Huang, K. and Fu, J. S.: Data Descriptor : A global gas flaring black carbon emission rate
680 dataset from 1994 to 2012, *Nature*, 1–11, doi:10.1038/sdata.2016.104, 2016.

681 Huang, K., Fu, J. S., Hodson, E. L., Dong, X., Cresko, J., Prikhodko, V. Y., Storey, J. M. and
682 Cheng, M. D.: Identification of missing anthropogenic emission sources in Russia:
683 Implication for modeling arctic haze, *Aerosol Air Qual. Res.*, 14(7), 1799–1811,
684 doi:10.4209/aaqr.2014.08.0165, 2014.

685 Ingvander, S., Rosqvist, G., Svensson, J. and Dahlke, H. E.: Seasonal and interannual
686 variability of elemental carbon in the snowpack of Storglaci??ren, northern Sweden, *Ann.*
687 *Glaciol.*, 54(62), 50–58, doi:10.3189/2013AoG62A229, 2013.

688 Jankowski, N., Schmidl, C., Marr, I. L., Bauer, H. and Puxbaum, H.: Comparison of methods
689 for the quantification of carbonate carbon in atmospheric PM10 aerosol samples, *Atmos.*
690 *Environ.*, 42(34), 8055–8064, doi:10.1016/j.atmosenv.2008.06.012, 2008.

691 Klimont, Z., Kupiainen, K., Heyes, C., Purohit, P., Cofala, J., Rafaj, P., Borcken-Kleefeld, J.
692 and Schöpp, W.: Global anthropogenic emissions of particulate matter including black
693 carbon, *Atmos. Chem. Phys. Discuss.*, (October), 1–72, doi:10.5194/acp-2016-880, 2016.

694 Lamarque, J. F., Shindell, D. T., Josse, B., Young, P. J., Cionni, I., Eyring, V., Bergmann, D.,
695 Cameron-Smith, P., Collins, W. J., Doherty, R., Dalsoren, S., Faluvegi, G., Folberth, G.,
696 Ghan, S. J., Horowitz, L. W., Lee, Y. H., MacKenzie, I. A., Nagashima, T., Naik, V.,
697 Plummer, D., Righi, M., Rumbold, S. T., Schulz, M., Skeie, R. B., Stevenson, D. S., Strode,
698 S., Sudo, K., Szopa, S., Voulgarakis, A. and Zeng, G.: The atmospheric chemistry and climate
699 model intercomparison Project (ACCMIP): Overview and description of models, simulations
700 and climate diagnostics, *Geosci. Model Dev.*, 6(1), 179–206, doi:10.5194/gmd-6-179-2013,
701 2013.

702 Law, K. S. and Stohl, A.: Arctic Air Pollution: Origins and Impacts, *Science* (80-.),
703 315(5818), 1537–1540, doi:10.1126/science.1137695, 2007.

704 Lelieveld, J., Evans, J. S., Fnais, M., Giannadaki, D. and Pozzer, A.: The contribution of
705 outdoor air pollution sources to premature mortality on a global scale., *Nature*, 525(7569),
706 367–71, doi:10.1038/nature15371, 2015.

707 Liu, J., Fan, S., Horowitz, L. W. and Levy, H.: Evaluation of factors controlling long-range
708 transport of black carbon to the Arctic, *J. Geophys. Res.*, 116(D4), D04307,
709 doi:10.1029/2010JD015145, 2011.

710 Macdonald, K. M., Sharma, S., Toom, D., Chivulescu, A., Hanna, S., Bertram, A., Platt, A.,
711 Elsasser, M., Huang, L., Chellman, N., McConnell, J. R., Bozem, H., Kunkel, D., Lei, Y. D.,
712 Evans, G. J. and Abbatt, J. P. D.: Observations of Atmospheric Chemical Deposition to High
713 Arctic Snow, *Atmos. Chem. Phys.*, 17, 5775–5788, doi:10.5194/acp-17-5775-2017, 2017.

714 McConnell, J. R., Edwards, R., Kok, G. L., Flanner, M. G., Zender, C. S., Saltzman, E. S.,

715 Banta, J. R., Pasteris, D. R., Carter, M. M. and Kahl, J. D. W.: 20th-Century Industrial Black
716 Carbon Emissions Altered Arctic Climate Forcing, *Science* (80-.), 317(5843), 1381–1384,
717 doi:10.1126/science.1144856, 2007.

718 Ogren, J. A., Charlson, R. J. and Groblicki, P. J.: Determination of elemental carbon in
719 rainwater, *Anal. Chem.*, 55(9), 1569–1572, doi:10.1021/ac00260a027, 1983.

720 Olivier, J. G. J., Aardenne, J. A. Van, Dentener, F. J., Pagliari, V., Ganzeveld, L. N. and
721 Peters, J. A. H. W.: Recent trends in global greenhouse gas emissions: regional trends 1970–
722 2000 and spatial distribution of key sources in 2000, *Environ. Sci.*, 2(2–3), 81–99,
723 doi:10.1080/15693430500400345, 2005.

724 Petzold, A., Ogren, J. A., Fiebig, M., Laj, P., Li, S. M., Baltensperger, U., Holzer-Popp, T.,
725 Kinne, S., Pappalardo, G., Sugimoto, N., Wehrli, C., Wiedensohler, A. and Zhang, X. Y.:
726 Recommendations for reporting black carbon measurements, *Atmos. Chem. Phys.*, 13(16),
727 8365–8379, doi:10.5194/acp-13-8365-2013, 2013.

728 Popovicheva, O. B., Evangelidou, N., Eleftheriadis, K., Kalogridis, A. C., Movchan, V.,
729 Sitnikov, N., Eckhardt, S., Makshtas, A. and Stohl, A.: Black carbon sources constrained by
730 observations and modeling in the Russian high Arctic, *Environ. Sci. Technol.*, submitted,
731 doi:10.1021/acs.est.6b05832, 2017.

732 Qi, L., Li, Q., Henze, D. K., Tseng, H.-L. and He, C.: Sources of Springtime Surface Black
733 Carbon in the Arctic: An Adjoint Analysis, *Atmos. Chem. Phys. Discuss.*, (February), 1–32,
734 doi:10.5194/acp-2016-1112, 2017.

735 Ruppel, M. M., Isaksson, I., Ström, J., Beaudon, E., Svensson, J., Pedersen, C. A. and
736 Korhola, A.: Increase in elemental carbon values between 1970 and 2004 observed in a 300-
737 year ice core from Holtedahlfonna (Svalbard), *Atmos. Chem. Phys.*, 14(20), 11447–11460,
738 doi:10.5194/acp-14-11447-2014, 2014.

739 Sand, M., Berntsen, T. K., von Salzen, K., Flanner, M. G., Langner, J. and Victor, D. G.:
740 Response of Arctic temperature to changes in emissions of short-lived climate forcers, *Nat.*
741 *Clim. Chang.*, 6(November), 1–5, doi:10.1038/nclimate2880, 2015.

742 Seibert, P. and Frank, A.: Source-receptor matrix calculation with a Lagrangian particle
743 dispersion model in backward mode, *Atmos. Chem. Phys.*, 4(1), 51–63, doi:10.5194/acp-4-
744 51-2004, 2004.

745 Sharma, S., Ishizawa, M., Chan, D., Lavoué, D., Andrews, E., Eleftheriadis, K. and
746 Maksyutov, S.: 16-year simulation of arctic black carbon: Transport, source contribution, and
747 sensitivity analysis on deposition, *J. Geophys. Res. Atmos.*, 118(2), 943–964,
748 doi:10.1029/2012JD017774, 2013.

749 Shiraiwa, M., Kondo, Y., Moteki, N., Takegawa, N., Sahu, L. K., Takami, A., Hatakeyama,
750 S., Yonemura, S. and Blake, D. R.: Radiative impact of mixing state of black carbon aerosol
751 in Asian outflow, *J. Geophys. Res. Atmos.*, 113(24), 1–13, doi:10.1029/2008JD010546, 2008.

752 Singh, P. and Haritashya, U. K.: *Encyclopedia of Snow, Ice and Glaciers.*, 2011.

753 Slinn, W. G. N.: Predictions for particle deposition to vegetative canopies, *Atmos. Environ.*,
754 16, 1785–1794, doi:10.1016/0004-6981(82)90271-2, 1982.

755 Stein, O., Flemming, J., Inness, A., Kaiser, J. W. and Schultz, M. G.: Global reactive gases
756 forecasts and reanalysis in the MACC project, *J. Integr. Environ. Sci.*, 8168(October 2014),
757 1–14, doi:10.1080/1943815X.2012.696545, 2012.

758 Stohl, A., Hittenberger, M. and Wotawa, G.: Validation of the lagrangian particle dispersion
759 model FLEXPART against large-scale tracer experiment data, *Atmos. Environ.*, 32(24),
760 4245–4264, doi:10.1016/S1352-2310(98)00184-8, 1998.

761 Stohl, A., Forster, C., Eckhardt, S., Spichtinger, N., Huntrieser, H., Heland, J., Schlager, H.,
762 Wilhelm, S., Arnold, F. and Cooper, O.: A backward modeling study of intercontinental
763 pollution transport using aircraft measurements, *J. Geophys. Res. Atmos.*, 108(D12), 4370,
764 doi:10.1029/2002JD002862, 2003.

765 Stohl, A., Forster, C., Frank, A., Seibert, P. and Wotawa, G.: Technical note: The Lagrangian
766 particle dispersion model FLEXPART version 6.2, *Atmos. Chem. Phys.*, 5(9), 2461–2474,
767 doi:10.5194/acp-5-2461-2005, 2005.

768 Stohl, A., Andrews, E., Burkhart, J. F., Forster, C., Herber, A., Hoch, S. W., Kowal, D.,
769 Lunder, C., Mefford, T., Ogren, J. A., Sharma, S., Spichtinger, N., Stebel, K., Stone, R.,
770 Ström, J., Tørseth, K., Wehrli, C. and Yttri, K. E.: Pan-Arctic enhancements of light
771 absorbing aerosol concentrations due to North American boreal forest fires during summer
772 2004, *J. Geophys. Res. Atmos.*, 111(22), 1–20, doi:10.1029/2006JD007216, 2006.

773 Stohl, A., Klimont, Z., Eckhardt, S., Kupiainen, K., Shevchenko, V. P., Kopeikin, V. M. and

774 Novigatsky, A. N.: Black carbon in the Arctic: The underestimated role of gas flaring and
775 residential combustion emissions, *Atmos. Chem. Phys.*, 13(17), 8833–8855, doi:10.5194/acp-
776 13-8833-2013, 2013.

777 Stohl, A., Aamaas, B., Amann, M., Baker, L. H., Bellouin, N., Berntsen, T. K., Boucher, O.,
778 Cherian, R., Collins, W., Daskalakis, N., Dusinska, M., Eckhardt, S., Fuglestvedt, J. S., Harju,
779 M., Heyes, C., Hodnebrog, Hao, J., Im, U., Kanakidou, M., Klimont, Z., Kupiainen, K., Law,
780 K. S., Lund, M. T., Maas, R., MacIntosh, C. R., Myhre, G., Myriokefalitakis, S., Olivie, D.,
781 Quaas, J., Quennehen, B., Raut, J. C., Rumbold, S. T., Samset, B. H., Schulz, M., Seland,
782 Shine, K. P., Skeie, R. B., Wang, S., Yttri, K. E. and Zhu, T.: Evaluating the climate and air
783 quality impacts of short-lived pollutants, *Atmos. Chem. Phys.*, 15(18), 10529–10566,
784 doi:10.5194/acp-15-10529-2015, 2015.

785 Svensson, J., Ström, J., Hansson, M., Lihavainen, H. and Kerminen, V.-M.: Observed metre
786 scale horizontal variability of elemental carbon in surface snow, *Environ. Res. Lett.*, 8(3),
787 34012, doi:10.1088/1748-9326/8/3/034012, 2013.

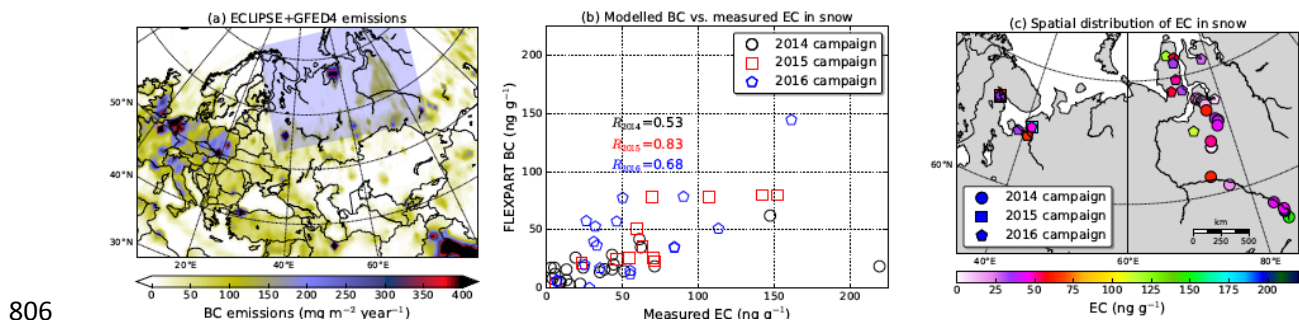
788 Turner, M. D., Henze, D. K., Capps, S. L., Hakami, A., Zhao, S., Resler, J., Carmichael, G.
789 R., Stanier, C. O., Baek, J., Sandu, A., Russell, A. G., Nenes, A., Pinder, R. W., Napelenok, S.
790 L., Bash, J. O., Percell, P. B. and Chai, T.: Premature deaths attributed to source-specific BC
791 emissions in six urban US regions, , 10(114014), doi:10.1088/1748-9326/10/11/114014/meta,
792 2005.

793 Wang, Q., Jacob, D. J., Fisher, J. A., Mao, J., Leibensperger, E. M., Carouge, C. C., Le Sager,
794 P., Kondo, Y., Jimenez, J. L., Cubison, M. J. and Doherty, S. J.: Sources of carbonaceous
795 aerosols and deposited black carbon in the Arctic in winter-spring: Implications for radiative
796 forcing, *Atmos. Chem. Phys.*, 11(23), 12453–12473, doi:10.5194/acp-11-12453-2011, 2011.

797 Warren, S. G. and Wiscombe, W. J.: A Model for the Spectral Albedo of Snow. II: Snow
798 Containing Atmospheric Aerosols, *J. Atmos. Sci.*, 37, 2734–2745, doi:10.1175/1520-
799 0469(1980)037<2734:AMFTSA>2.0.CO;2, 1980.

800 Winiger, P., Andersson, A., Eckhardt, S., Stohl, A., Semiletov, I. P., Dudarev, O. V., Charkin,
801 A., Shakhova, N., Klimont, Z., Heyes, C. and Gustafsson, Ö.: Siberian Arctic black carbon
802 sources constrained by model and observation, *Proc. Natl. Acad. Sci.*, 1–8,
803 doi:10.1073/pnas.1613401114, 2017.

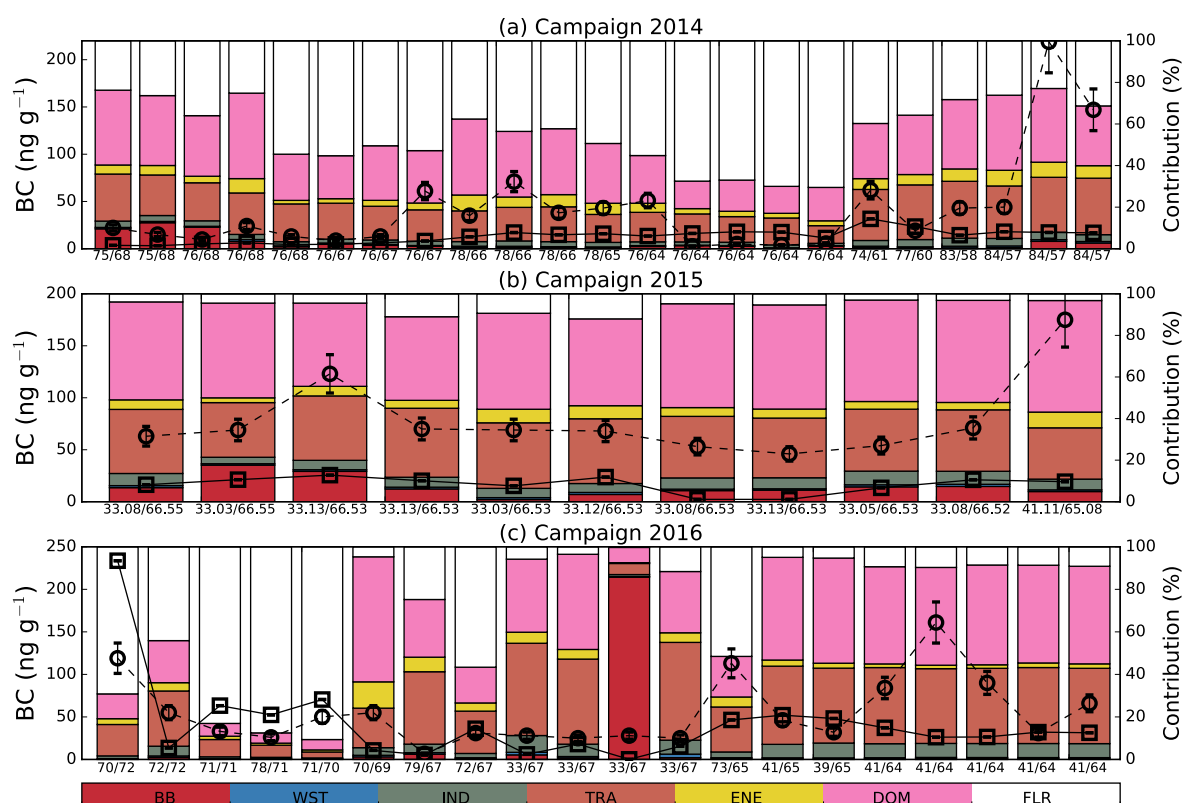
805 **FIGURE CAPTIONS FOR MANUSCRIPT**



807 **Figure 1.** (a) Total emissions of BC (anthropogenic emissions from ECLIPSE (Klimont et al.,
 808 2016) and biomass burning from GFED4 (Giglio et al., 2013). The blue shade shows the area
 809 of interest that is zoomed on the right. (b) Comparison of modelled BC concentrations in
 810 snow with measured EC concentrations. (c) Spatial distribution of EC in snow measured by
 811 thermal optical analysis (TOA) of filtered snow samples from northwestern European Russia
 812 and Western Siberia in spring–time 2014, 2015 and 2016.

813

SOURCE CONTRIBUTION TO SNOW BC

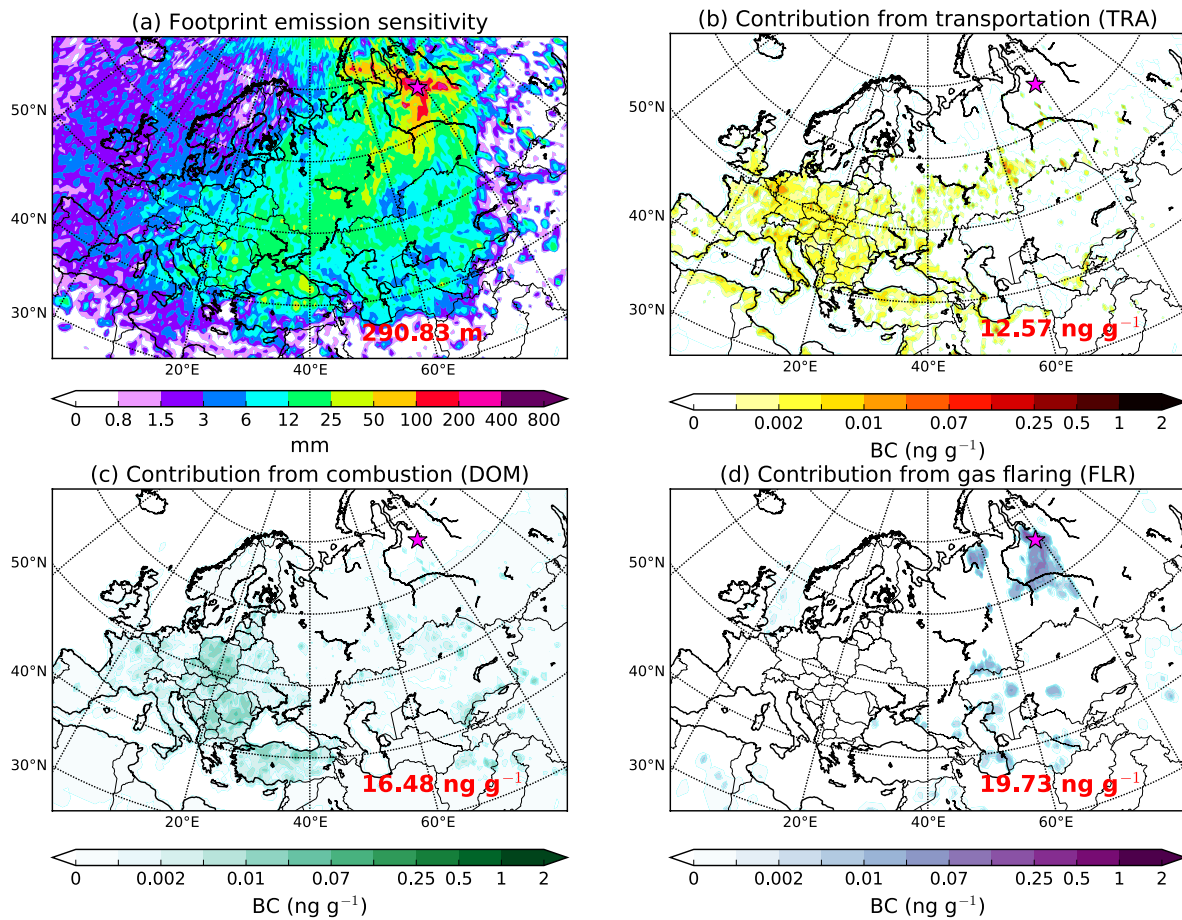


814

815 **Figure 2.** Contribution from the various emission categories considered in the ECLIPSE and
 816 GFED inventories to simulated BC concentrations in snow in (a) 2014, (b) 2015 and (c) 2016
 817 in Western Siberia and northwestern European Russia. BB stands for biomass burning, WST
 818 for waste burning, IND for industrial combustion and processing, TRA for surface
 819 transportation, ENE for emissions from energy conversion, and extraction, DOM for
 820 residential and commercial combustion, and FLR for gas flaring. Bars show the relative
 821 source contribution (0 –100%, right axis) and are sorted, from left to right, from the
 822 northernmost to the southernmost measurement location (coordinates are reported on the
 823 bottom as longitude/latitude). Measured EC concentrations in snow are reported with open
 824 circles, whereas modelled BC is shown with open rectangles (left axis).

825

**EMISSION SENSITIVITY AND SOURCE CONTRIBUTION TO SNOW BC IN 2014
(78.17° E - 65.78° N)**

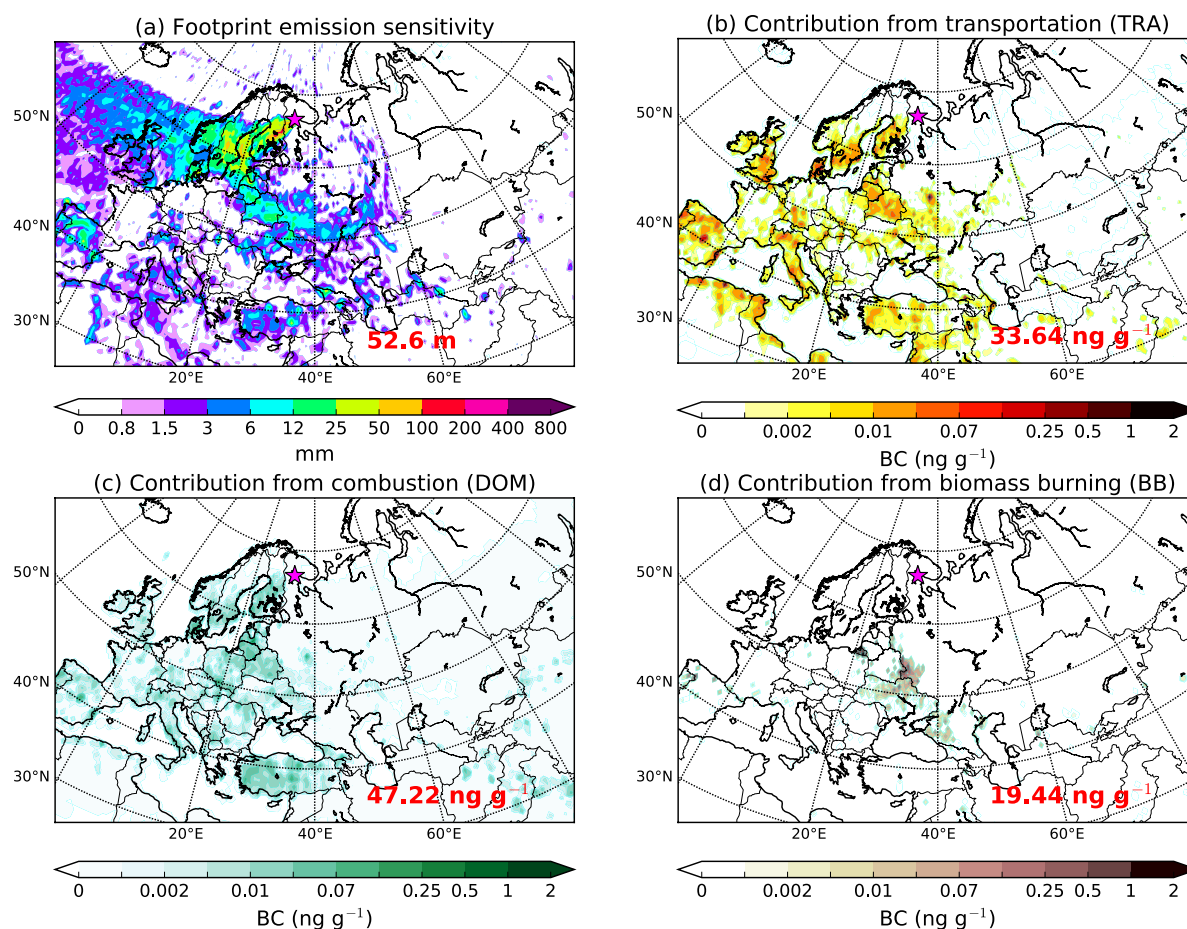


826

827 **Figure 3.** (a) FLEXPART emission sensitivity, contribution from (b) transportation (TRA),
 828 (c) residential and commercial combustion (DOM) and (d) gas flaring (FLR) to the maximum
 829 measured concentration of snow EC recorded along the transect from Tomsk to Yamal
 830 Peninsula in Western Siberia during the campaign of 2014.

831

**EMISSION SENSITIVITY AND SOURCE CONTRIBUTION TO SNOW BC IN 2015
(33.13° E - 66.53° N)**

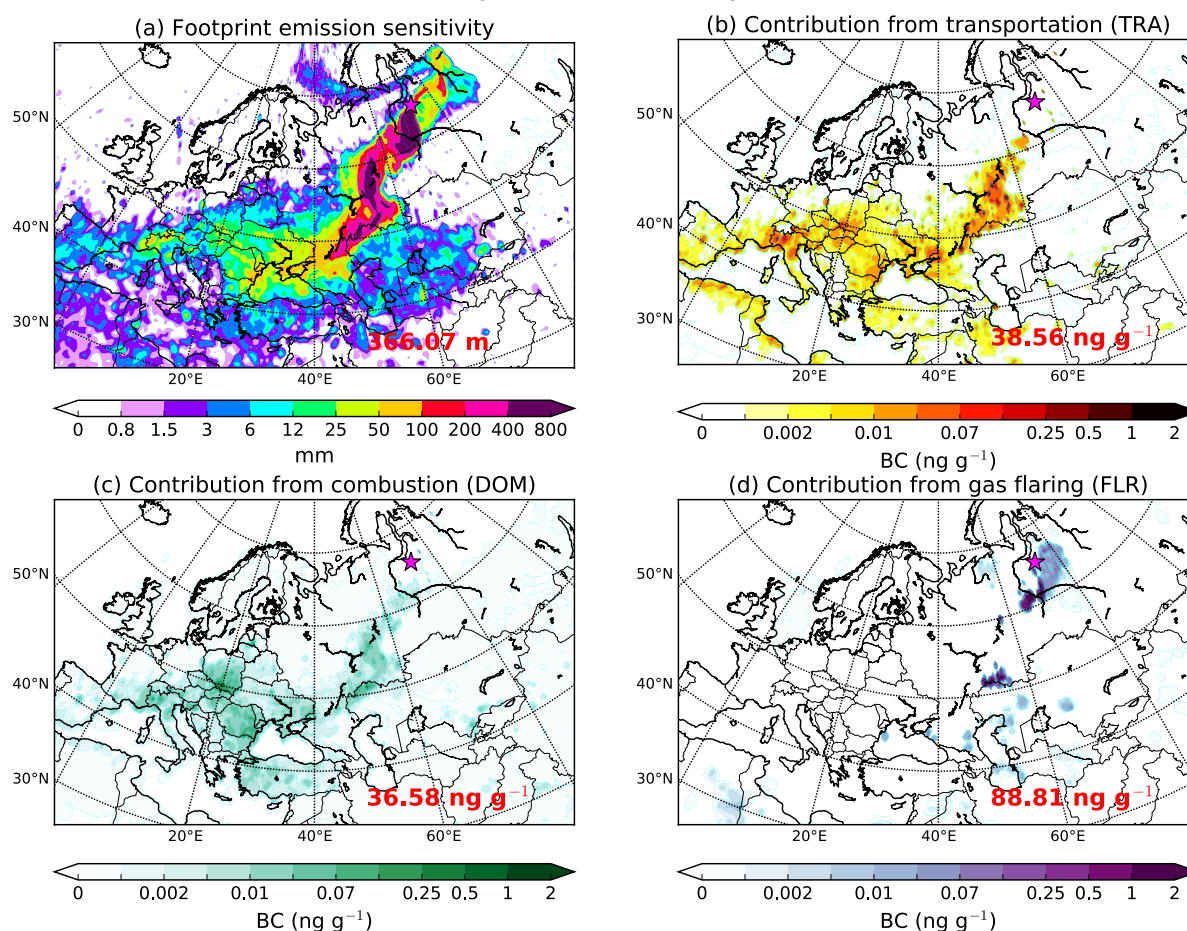


832

833 **Figure 4.** (a) FLEXPART emission sensitivity, (b) contribution from transportation (TRA),
 834 (c) residential and commercial combustion (DOM) and (d) gas flaring (FLR) to the maximum
 835 measured concentration of snow EC recorded in northwestern European Russia (Kindo
 836 Peninsula and Arkhangelsk region) during the campaign of 2015.

837

**EMISSION SENSITIVITY AND SOURCE CONTRIBUTION TO SNOW BC IN 2016
(72.94° E - 65.36° N)**

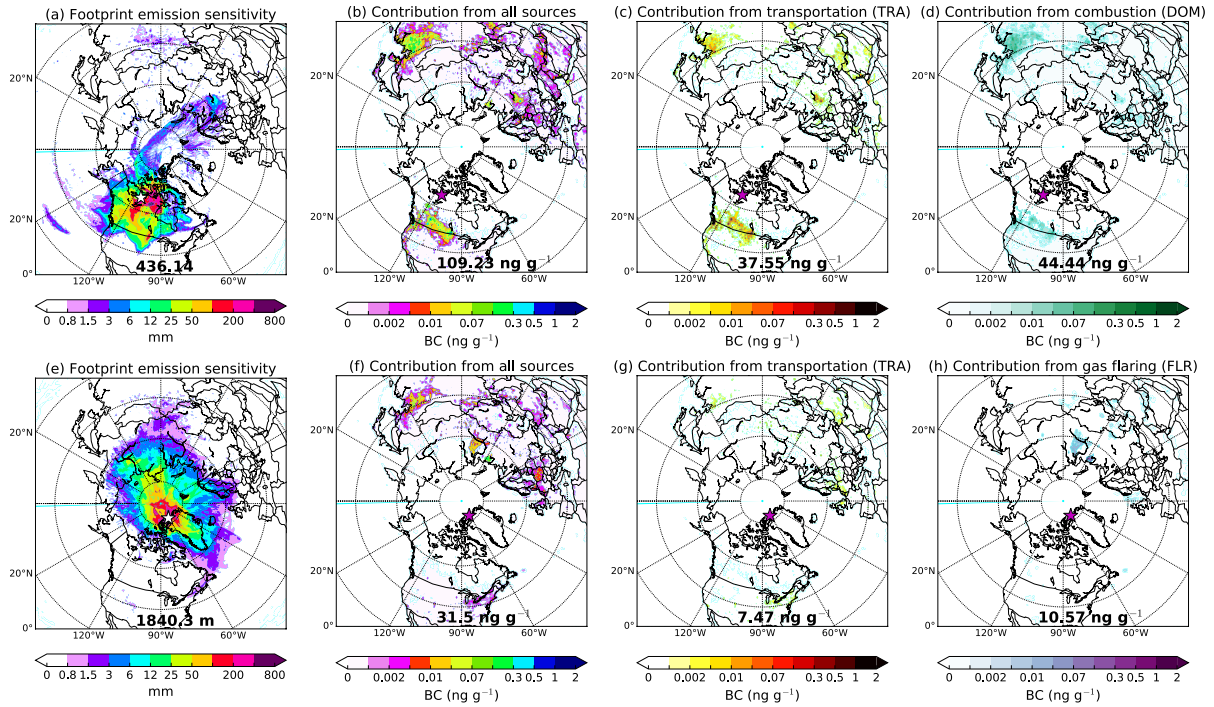


838

839 **Figure 5.** (a) FLEXPART emission sensitivity and (b) contribution from transportation
 840 (TRA), (c) residential and commercial combustion (DOM) and (d) gas flaring (FLR) to the
 841 maximum measured concentration of snow EC recorded in Kindo Peninsula, Arkhangelsk and
 842 Yamal Peninsula (northwestern European Russia, Western Siberia) during the campaign of
 843 2016.

844

**EMISSION SENSITIVITY AND SOURCE CONTRIBUTION TO SNOW BC
(CANADIAN ARCTIC 2007 - ALERT 2014-2015)**

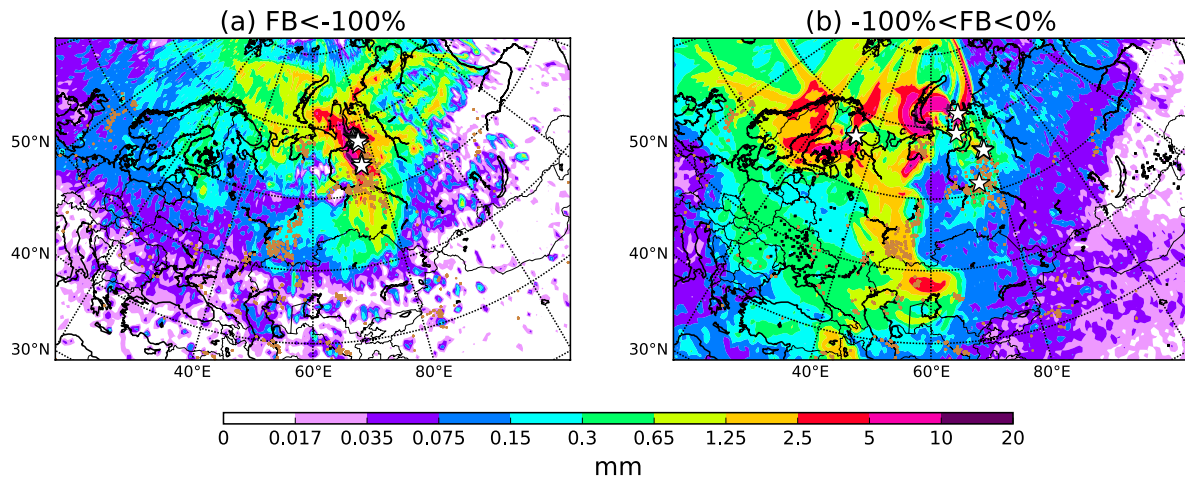


845

846 **Figure 6.** (a–d) Footprint emission sensitivity and major contribution from all sources, TRA
 847 and DOM averaged for the samples that showed overestimated modelled concentrations of
 848 BC in 2007 (Doherty et al., 2010). (e–h) Footprint emission sensitivity and contribution from
 849 all sources, TRA and FLR for the samples collected in Alert (Macdonald et al., 2017) that
 850 model overestimated by more than three times.

851

**AVERAGE FOOTPRINT EMISSION SENSITIVITY
NORMALISED AGAINST UNDERESTIMATION FROM OBSERVATIONS**



852

853 **Figure 7.** (a) Footprint emission sensitivity from FLEXPART averaged for the sampling
854 points where the model underestimated observations significantly ($FB < -100\%$) and (b)
855 less significantly ($-100\% < FB < 0\%$). Black squares show the locations of active fires
856 detected by MODIS (Moderate Resolution Imaging Spectroradiometer) (Giglio et al., 2003).
857 Brown dots show the location of gas flaring sites from the Global Gas Flaring Reduction
858 Partnership (GGFR) (<http://www.worldbank.org/en/programs/gasflaringreduction>).

859

860 **FIGURE CAPTIONS FOR SUPPLEMENTS**

861

862 **Figure S 1.** Fractional bias ($FB = [(C_m - C_o)/(C_m + C_o) \times 0.5] \times 100\%$) for all samples
863 collected from the three campaigns in Western Siberia and northwestern European Russia in
864 2014, 2015 and 2016. MFB (mean fractional bias) is the fractional bias averaged for all snow
865 samples from 2014, 2015 and 2016, whereas RMSE is the root mean square error in ng g^{-1} .

866 **Figure S 2.** (a) Distribution of snow measurements of BC adopted from Doherty et al. (2010)
867 in the Arctic from 2005 to 2009. (b) Simulated (FLEXPART) BC concentrations in snow for
868 the same period (right). MFB, RMSE and correlation coefficient (R) values are further given.

869 **Figure S 3.** Timeseries of simulated and measured BC concentrations in snow collected in
870 Alert (Macdonald et al., 2017). Correlation coefficient (R) between modelled and measured
871 BC, RMSE and MFB values are also shown.

872 **Figure S 4.** (a) Average footprint emission sensitivity and (b–f) source contribution (from all
873 sources, TRA, DOM, FLR and BB) for all the samples located in northwestern European
874 Russia.

875 **Figure S 5.** (a) Average footprint emission sensitivity and (b–f) source contribution (from all
876 sources, TRA, DOM, FLR and BB) for all the samples located in Western Siberia (north of 62
877 °N).

878 **Figure S 6.** (a) Average footprint emission sensitivity and (b–f) source contribution (from all
879 sources, TRA, DOM, FLR and BB) for all the samples located in Western Siberia (south of
880 62 °N).